VARIATIONAL ASSIMILATION OF FLUID MOTION FROM IMAGE SEQUENCE

NICOLAS PAPADAKIS* AND ÉTIENNE MÉMIN†

Abstract. In this paper, a variational technique derived from optimal control theory is used in order to realize a dynamically consistent motion estimation of a whole fluid image sequence. The estimation is conducted through an iterative process involving a forward integration of a given dynamical model followed by a backward integration of an adjoint evolution law. By combining physical conservation laws and image observations, a physically grounded temporal consistency is imposed and the quality of the motion estimation is significantly improved. The method is validated on two synthetic image sequences provided by numerical simulation of fluid flows and on real world meteorological examples.

Key words. Optimal control, dense motion estimation, fluid motion, data assimilation

1. Introduction. The analysis of complex fluid flows is a very challenging issue in numerous scientific domains. In that prospect, flow visualization and extraction of accurate kinetic or dynamical measurements are of the utmost importance. Since several years, the study of dynamic structures and the estimation of dense velocity fields from fluid image sequences have received a great attention from the computer vision community [7, 11, 12, 19, 25, 38, 39]. Application domains range from experimental visualization in fluid mechanics to geophysical flow analysis in environmental sciences (meteorology, climatology, oceanography, ...). In particular, accurate measurements of atmospheric flow dynamics is a very important piece of information for weather forecasting, climate prediction or climate evolution analysis, etc... Such an interest can be extended to the analysis of very complex situation involving unknown boundary conditions, multi-phase fluids or fluid structures interactions, in which information brought by image data may be a very interesting alternative to the numerical simulation of pure physical modeling.

As a matter of fact, even though it is generally possible to provide an accurate modeling of the large scales of an experimental flow, the small motion scales are much more difficult to reproduce accurately. In this regard, image observation have the advantage to represent inherently a large range of the motion scales of the observed flow. The coupling of fluid dynamical models, simulation techniques and image data measurements appears consequently to be a very appealing approach for the reconstruction, or the accurate measurement of fluid flows. In this paper we introduce a generic technique allowing such coupling between image data and a dynamical model.

The analysis of fluid motion through image sequences is particularly challenging in several application contexts due to the low contrast of the luminance function and its variations generated by the fluid motion. For these reasons, motion analysis techniques designed for computer vision applications and quasi-rigid motions are generally not well adapted in this context. Methods for fluid-dedicated dense estimation have been proposed to estimate fluid motion [7, 8, 17, 38] or to characterize the principal structures of the flow [9]. However, these motion estimators are still using only a small set of images and thus may suffer from a temporal inconsistency from frame

*Barcelona Media/Univesitat Pompeu Fabra, Carrer Ocata 1, O8003 Barcelona - Spain, (nicolas.papadakis@gmail.com)

†INRIA Bretagne-Atlantique, Campus de Beaulieu 35042 Rennes Cedex - France, (memin@irisa.fr)

to frame. The design of appropriate methods enabling to take into account the underlying physics of the observed flow constitutes a widely open domain of research. Even if some spatio-temporal estimators have been proposed [2, 4, 26, 37] in computer vision, they all relies on simple stationary assumption and none of them enable to enforce a global coherency of the estimates with respect to the dynamics of the observed phenomena. Imposing such a dynamical constraint is particularly attractive for the accurate velocity measurement of complex flows and to guarantee a temporal consistency of the velocity fields trajectory.

Recently, new approaches relying on the *vorticity-velocity* formulation of *Navier-Stokes* equations have been proposed [16, 33]. These estimators include a prediction term based on this conservation law that enables to impose a goodness fit between the current estimation and a predicted one [16, 33]. Even if these techniques enforces a temporal coherency, the set of final estimates provided along the sequence does not however necessarily respect the considered fluid conservation laws. They just impose from time to time a clever initialization for the motion estimation process. If for any reasons, at a given time, the estimator fails to supply an estimate that is close enough to the actual solution, this current estimate will be propagated from time to time and an increasing drift of the estimated trajectory will observed. This is due to the fact that those predictive estimators do not correspond to the settling of a global spatio-temporal optimal strategy.

In this work, we propose to define the motion estimation problem through variational assimilation principles related to optimal control theory [20, 22] and used in geophysical sciences [1,20,36]. These techniques enable, in the same spirit as a Kalman filter, a temporal smoothing along the whole image sequence. As a Bayesian smoother, they combine a dynamical evolution law of the flow state variables of interest with the whole set of available related noisy measurements. Nevertheless, unlike known stochastic filtering implementation, variational assimilation techniques allows to cope naturally with state spaces of very large dimension. As opposed for instance to the stochastic filter proposed in [10] which aims at describing and tracking only the main structures of the flow, the objective is here to measure and track an extended range of the flow scales.

The approach we propose is expressed as the minimization of a global spatio-temporal functional modeling the integrated discrepancy along time between the features trajectory and photometric measurements. The associated optimization process is led through the introduction of *adjoint techniques* borrowed to optimal control theory [22, 23]. This method has the advantage to provide an efficient expression of the functional gradient. This is particularly interesting when the functional gradients can hardly be numerically computed through finite differences.

Thanks to the dynamics introduced to describe the motion fields evolution, the functionals we will consider do not incorporate any additional smoothing functions to discard ambiguities or to recover the motion of low photometric gradient areas. These kinds of regularizers used in any variational dense motion schemes and that remains always questionable from the point of view of the physics of the observed phenomenon are not required here.

This paper is organized as follows. The principle of the optimal control theory used in this work is introduced in section 2. The process is applied to the recovery of fluid motion in section 3. The discretization schemes used are detailed in section 4.1 and finally, numerical experiments are presented in section 5. This work corresponds to a detailed version of two conference papers [29, 30]. It also follows a work pro-

posed for the filtering of noisy motion fields [31]. We will however give here another presentation of the adjoint optimization technique.

Let us note that a related work using optimal control has been proposed for the estimation of dense motion fields in image sequences [3]. However, the method is dedicated to the recovering of stationary rigid motion and involved a simple observation model. In addition, unlike the approach we propose, this technique includes, in the same way as traditional motion estimator, explicit spatial *a priori* smoothing functional. Such regularization terms have the drawback to introduce smoothness constraints which are not physically grounded and leads to biased solutions in areas of low photometric contrasts. Another technique relying on optimal control has been proposed in [32]. This technique operates on two consecutive images and relies on a Stokes flow conservation law model – in which the effect of the non linear advection term of the Navier-Stokes equation is neglected.

2. Data assimilation. In this section we will first describe the general framework proposed for a dynamically consistent estimation issues. It relies on variational data assimilation concepts [1, 20, 36] proposed for the analysis of geophysical flows.

2.1. Definition. Data assimilation is a technique based on optimal control theory [23] that enables to perform the estimation over time of state variables representing a system of interest. A smoothing is done according to an initial state, a dynamic law and noisy measurements. This setting shares the same aim as a Bayesian smoother such as the Kalman filter used within a forward-backward filtering (i.e batch mode). Nevertheless, this framework allows to handle very large scale systems and is thus intensively used in environmental sciences [1, 20, 36] for atmospheric flows or oceanic simulations. We rely on this technique to estimate in batch mode the complete trajectories along an image sequence of curves and motion fields. The data assimilation setting is basically composed of an ideal dynamical model of the target system, an initialization of the system's state and an observation equation which relates the system variables to some measurements:

$$\begin{cases} \partial_t X + \mathbb{M}(X) = \nu(x,t) \\ X(x,t_0) = X_0(x) + \eta(x) \\ Y(x,t) = \mathbb{H}(X(x,t)) + \epsilon(x,t). \end{cases} \tag{2.1}$$

The right hand side of the first equation describes, through a differential operator $\mathbb{M}$, the evolution of the state function X defined over the image plane Ω and the whole image sequence time range $[t_0; t_f]$. In our case, the components of this vectorial function will include a motion field representations. This will be further detailed in the next section, but for sake of generality, let us first consider a general state function. The second equation sets up an initial condition for the state function through a given initialization $X_0(x)$. The last equation links an observation function $Y(x,t)$, constituted by noisy measurements of the state function components, to the state function . This relation is formalized through a differential operator $\mathbb{H}$. The observation function is usually composed of discrete and sparse measurements. In these three equations ν, η and ϵ are time varying control functions defined on the whole image plane. They are respectively associated to covariance matrices $Q(x,t,x',t')$, $B(x,x')$ and $R(x,t,x',t')$. These functions represent the errors involved in the different components of the system (i.e dynamical model errors, initialization errors and measurement errors).

2.2. Penalty function. The system of equations (2.1) could be as well specified through three Gaussian conditional probability densities $p(X|X(0))$, $p(X(0)|X_0)$ and

$p(Y|X)$ related respectively to the state trajectory X along time to the initial state value $X(0)$, the initial state value to the initial condition X_0 and Y, the complete set of measurements to the state X. As in any stochastic filtering problem, we aim here at estimating the conditional expectation of the state trajectory given the whole set of available observations (here the complete sequence of observations). As all the pdf involved here are Gaussian, this comes to seeking for the mode of the *a posteriori* distribution $p(X|Y, X_0)$. Such a maximum a posteriori estimation leads then to the minimization of a quadratic functional defined as:

$$\begin{aligned} J(X) &= \frac{1}{2}\int_{\Omega}\int_{\Omega} \left(X(x,t_0) - X_0(x)\right)^T B^{-1}(x,x') \left(X(x',t_0) - X_0(x')\right) dx'dx \\ &+ \frac{1}{2}\int_{\Omega,t}\int_{\Omega,t} \left(\partial_t X + \mathbb{M}(X)\right)^T(x,t) Q^{-1}(x,t,x',t') \left(\partial_t X + \mathbb{M}(X)\right)(x',t') dt'dx'dtdx \\ &+ \frac{1}{2}\int_{\Omega,t}\int_{\Omega,t} \left(Y - \mathbb{H}(X)\right)^T (x,t) R^{-1}(x,t,x',t') \left(Y - \mathbb{H}(X)\right)(x',t') dt'dx'dtdx, \end{aligned} \tag{2.2}$$

where

$$\int_{\Omega,t} = \int_{\Omega}\int_{t_0}^{t_f}.$$

Few remarks can be done here. The covariance functions Q and R which appear in the functional above may link any point of the spatio-temporal domain. Nevertheless, if any two points are uncorrelated the double space-time integral involved simplifies in a single integral (i.e. functions Q and R are only function of x and t, and B is only a function of x). Their associated discretization corresponds then to diagonal matrices. Even if at the end, we will rely on such assumption, we wish to stay first in the most general case. This functional and the covariance functions involved in the previous functional ensue from the assumption of an inexact dynamical law together with noisy measurements and inaccurate initial conditions. Let us also remark that in the most usual cases, the variational data assimilation techniques used in environmental sciences relies on an exact version of the state evolution law (i.e. without any model error). In this latter case the second line of the functional (the model part) disappears. The functional then depends only on the initial condition, and comes to an initial value control problem. Interested readers may found a presentation of this setup for image processing problems in [31]. A perfect modeling seems to us irrelevant in image analysis since the different models on which we can rely on are usually inaccurate due for instance to 3D-2D projections, varying lighting conditions, completely unknown boundary conditions, etc ... Considering an incertitude term on the dynamical model, we therefore somewhat move apart from the traditional setting. Despite this difference, we will nevertheless rely on the same *adjoint* optimization principles [20,36] to minimize the functional.In the following we give a presentation of this principle that is slightly different from the one given in [31]. It relies here on the direct computation of the Euler-Lagrange optimality condition through an additional adjoint variable.

A minimizer X of functional J is also a minimizer of a cost function $J(X + \beta\theta(x,t))$, where $\theta(x,t))$ belongs to a space of admissible function and β is a positive parameter. In other words, X must cancel out the directional derivative:

$$\partial_X J(\theta) = \lim_{\beta\to 0} \frac{dJ(X + \beta\theta(x,t))}{d\beta} = 0.$$

$J(X+\beta\theta(x,t))$ may be written as:

$$\begin{aligned} J &= \frac{1}{2}\int_\Omega\int_\Omega (X+\beta\theta-X_0)^T B^{-1}(X+\beta\theta-X_0)dx'dx \\ &+ \frac{1}{2}\int_{\Omega,t} (\partial_t X+\beta\partial_t\theta+\mathbb{M}(X+\beta\theta))^T \int_{\Omega,t} Q^{-1}(\partial_t X+\beta\partial_t\theta+\mathbb{M}(X+\beta\theta))\,dt'dx'dtdx \\ &+ \frac{1}{2}\int_{\Omega,t}\int_{\Omega,t} (Y-\mathbb{H}(X+\beta\theta))^T R^{-1}(Y-\mathbb{H}(X+\beta\theta))dt'dx'dtdx. \end{aligned} \tag{2.3}$$

2.3. Adjoint variable. In order to perform an integration by part – to factorize this expression by θ– we introduce an "adjoint variable" λ defined by:

$$\lambda(x,t) = \int_{\Omega,t} Q^{-1}\left(\partial_t X+\mathbb{M}(X)\right)dt'dx', \tag{2.4}$$

as well as *linear tangent operators* $\partial_X\mathbb{M}$ and $\partial_X\mathbb{H}$ defined by:

$$\lim_{\beta\to 0}\frac{d\mathbb{M}(X+\beta\theta)}{d\beta} = \partial_X\mathbb{M}\theta. \tag{2.5}$$

Such linear operators corresponds to the Gâteaux derivative at point X of the operators $\mathbb{M}$ and $\mathbb{H}$. Let us note that the derivative of a linear operator is the operator itself. By taking the limit $\beta\to 0$, the derivative of expression (2.3) then reads

$$\begin{aligned} \lim_{\beta\to 0}\frac{dJ}{d\beta} &= \int_\Omega\int_\Omega \theta^T(x,t_0)B^{-1}(X(x',t_0)-X_0(x'))dx'dx \\ &+ \int_{\Omega,t}(\partial_t\theta+\partial_X\mathbb{M}\theta)^T(x,t)\lambda(x,t)dtdx \\ &- \int_{\Omega,t}\int_{\Omega,t}(\partial_X\mathbb{H}\theta)^T(x',t')R^{-1}(Y-\mathbb{H}(X))dt'dx'dtdx \\ &= 0. \end{aligned} \tag{2.6}$$

Considering the three following integrations by parts, we can get rid of the partial derivatives of the admissible function θ in expression (2.6), i.e.

$$\int_{\Omega,t}\partial_t\theta^T\lambda(x,t)dtdx = \int_\Omega \theta^T(x,t_f)\lambda(x,t_f)dx - \int_\Omega \theta^T(x,t_0)\lambda(x,t_0)dx - \int_{\Omega,t}\theta^T(x,t)\partial_t\lambda dtdx, \tag{2.7}$$

$$\int_{\Omega,t}(\partial_X\mathbb{M}\theta)^T\lambda(x,t)dtdx = \int_{\Omega,t}\theta^T\partial_X\mathbb{M}^*\lambda(x,t)dtdx, \tag{2.8}$$

$$\int_{\Omega,t}\int_{\Omega,t}(\partial_X\mathbb{H}\theta)^T R^{-1}(Y-\mathbb{H}(X))dt'dx'dtdx = \int_{\Omega,t}\int_{\Omega,t}\theta^T\partial_X\mathbb{H}^*R^{-1}\left(Y-\mathbb{H}(X)\right)dt'dx'dtdx. \tag{2.9}$$

In the two last equations, we have introduced adjoint operators $\partial_X\mathbb{M}^*$ and $\partial_X\mathbb{H}^*$ as compact notations of the integration by parts of the associated linear tangent operators. Writing $\langle X,Y\rangle$ the scalar product in $L^2(\Omega)$, this reads more compactly as:

$$\langle\partial_X\mathbb{M}X_1,X_2\rangle_X = \langle X_1,\partial_X\mathbb{M}^*X_2\rangle_X \qquad \langle\partial_X\mathbb{H}X,Y\rangle_Y = \langle X,\partial_X\mathbb{H}^*Y\rangle_X. \tag{2.10}$$

Gathering all the elements we have so far, equation (2.6) can be rewritten as:

$$\begin{aligned}\lim_{\beta\to 0}\frac{dJ}{d\beta} =& \int_\Omega \theta^T(x,t_f)\lambda(x,t_f)dx + \int_\Omega \theta^T(x,t_0)\Big[\int_\Omega \left(B^{-1}(X(x',t_0)-X_0(x')) - \lambda(x,t_0)\right)dx'\Big]dx \\ &+ \int_{\Omega,t}\theta^T\left[(-\partial_t\lambda + \partial_X\mathbb{M}^*\lambda) - \int_{\Omega,t}\partial_X\mathbb{H}^*R^{-1}(Y-\mathbb{H}(X))dt'dx'\right]dtdx \\ &= 0.\end{aligned} \tag{2.11}$$

2.4. Forward/backward equations. Since the functional derivative must be null for any arbitrary independent admissible functions in the three integrals of expression (2.11), all the other members appearing in the three integral terms must be identically null. It follows a coupled system of forward and backward PDE's with initial and final conditions:

$$\lambda(x,t_f) = 0, \tag{2.12}$$

$$-\partial_t\lambda + \partial_X\mathbb{M}^*\lambda = \int_{\Omega,t}\partial_X\mathbb{H}^*R^{-1}(x,t,x',t')(Y-\mathbb{H}(X))dt'dx', \tag{2.13}$$

$$\lambda(x,t_0) = \int_\Omega \left(B^{-1}(x,x')(X(x',t_0)-X_0(x')\right)dx', \tag{2.14}$$

$$\partial_t X(x,t) + \mathbb{M}(X(x,t)) = \int_{\Omega,t} Q(x,t,x',t')\lambda(x',t')dt'dx'. \tag{2.15}$$

The forward equation (2.15) corresponds to the definition of the adjoint variable (2.4) and has been obtained introducing Q, the pseudo-inverse of Q^{-1}, defined as [1]:

$$\int_{\Omega,t} Q(x,t,x',t')Q^{-1}(x',t',x'',t'')dt'dx' = \delta(x-x'')\delta(t-t'').$$

Let us remark that if the model is assumed to be perfect, we would have $Q = 0$ and retrieve the case of a perfect dynamical state model. Otherwise, equation (2.12) constitutes an explicit end condition for the adjoint evolution model equation (2.13). This adjoint evolution model can be integrated backward from the end condition assuming the knowledge of an initial guess for X to compute the discrepancy $Y-\mathbb{H}(X)$. To perform this integration, we also need to have an expression of the *adjoint evolution operator*. Let us recall that this operator is defined from an integration by part of the *linear tangent operator* associated to the evolution law operator. The analytic expression of such an operator is obviously not accessible in general. Nevertheless, it can be noticed that a discrete expression of this operator can be easily obtained from the discretization of the linear tangent operator. As a matter of fact, the adjoint of the linear tangent operator discretized as a matrix simply consists of the transpose of that matrix. Knowing a first solution of the adjoint variable, an initial update condition for the state variable can be obtained from (2.14) and a pseudo-inverse expression of the covariance matrix B. From this initial condition, equation (2.15) can be finally integrated forward.

It can also be noticed that equation (2.15) provides at convergence an expression of the model error:

$$\nu(x,t) = \int_{\Omega,t} Q(x,t,x',t')\lambda(x',t')dt'dx'. \tag{2.16}$$

Thus, the knowledge of the adjoint variable enables to estimate the error associated to the state variable evolution law. This may be sometimes useful to validate or invalidate a tracking result, or at least to infer some confidence measures on the result obtained.

2.5. Incremental state function. The previous system can be slightly modified to rely on an adequate initial guess for the state function. Considering a function of state increments linking the state function and an initial condition function, $\delta X = X - X_0$, and linearizing the operator $\mathbb{M}$ around the initial condition function X_0 [1]:

$$\mathbb{M}(X) = \mathbb{M}(X_0) + \partial_{X_0}\mathbb{M}(\delta X)$$

enables to split equation (2.15) into two pde's with an explicit initial condition:

$$X(x, t_0) = X_0(x), \tag{2.17}$$

$$\partial_t X_0 + \mathbb{M}(X_0) = 0, \tag{2.18}$$

$$\partial_t \delta X + \partial_{X_0}\mathbb{M}\delta X = \int_{\Omega,t} Q(x, t, x', t')\lambda(x', t')dt'dx'. \tag{2.19}$$

Combining equations (2.12-2.14) and (2.17-2.19) leads to the final tracking algorithm. The method first consists of a forward integration of the initial condition X_0 with the system's dynamical model equation (2.18). The current solution is then corrected by performing a backward integration (2.12, 2.13) of the adjoint variable. The evolution of λ is guided by a discrepancy measure between the observation and the estimate: $Y - \mathbb{H}(X)$. The initial condition is then updated through equation (2.14) and a forward integration of the increment δX is realized through the equation (2.19). The overall process is iteratively repeated until convergence. A sketch of the whole process is summarized in Algorithm (2.1).

ALGORITHM 2.1. *Let $X(t_0) = X_0$.*
(i) *From $X(t_0)$, compute $X(t)$, $\forall t \in]t_0, t_f[$ with a forward integration of system (2.18).*
(ii) *$X(t)$ being given, realize a backward integration of the adjoint variable with the system (2.13).*
(iii) *Compute the initial value of the incremental function(2.14).*
(iv) *From $dX(t_0)$, compute $dX(t)$, $\forall t \in]t_0, t_f[$ with a forward integration of system (2.19).*
(v) *Update $X = X + dX$.*
(vi) *Return to* (ii) *and repeat until convergence.*

3. Application to fluid motion tracking. We aim here at applying the previous framework for a consistent tracking along time of fluid motion velocity fields. For fluid flows, the Navier-Stokes equation provides a universal general law for predicting the evolution of the flow. The purpose will be thus to incorporate into a data assimilation process such a dynamical model together with noisy velocity measurements.

[1] The linearized operator includes as second member the Gâteaux derivative defined in (2.5)

3.1. Basic definitions. In this work, the formulation of the Navier-Stokes equation on which we will rely on uses the vorticity ξ and the divergence ζ of a 2D motion field $\boldsymbol{w} = [u, v]^T$ defined on the image domain Ω:

$$\begin{aligned}\xi &= \nabla^{\perp} \cdot \boldsymbol{w} = v_x - u_y,\\ \zeta &= \nabla \cdot \boldsymbol{w} = u_x + v_y.\end{aligned}$$

The vorticity is related to the presence of a rotating motion, whereas the divergence is related to the presence of sinks and sources in a flow. Assuming $\boldsymbol{w}$ vanishes at infinity[2], the vector field is decomposed using the orthogonal Helmholtz decomposition, as a sum of two potential functions gradient: $\boldsymbol{w} = \nabla^{\perp}\Psi + \nabla\Phi$. The stream function Ψ and the velocity potential Φ respectively correspond to the solenoidal and the irrotational part of the vector field $\boldsymbol{w}$. They are linked to the divergence and vorticity maps through two Poisson Equations: $\xi = \Delta\Psi$ and $\zeta = \Delta\Phi$. Expressing the solution of both equations as a convolution product with the Green kernel $G(x) = \frac{1}{2\pi}\ln(|x|)$ associated to the 2D Laplacian operator:

$$\begin{aligned}\Psi &= G * \xi\\ \Phi &= G * \zeta,\end{aligned} \tag{3.1}$$

the whole velocity field can be recovered knowing its divergence and vorticity:

$$\boldsymbol{w} = \nabla^{\perp} G * \xi + \nabla G * \zeta. \tag{3.2}$$

As this relation involves convolution products, the computation can be efficiently implemented in the Fourier domain.

3.2. Fluid motion evolution equation. In order to consider a tractable expression of the Navier-Stokes equation for the tracking problem, we rely in this work on the 2D vorticity-velocity formulation of the 3D incompressible Navier-Stokes equation, as obtained in the shallow water model:

$$\partial_t \xi + \boldsymbol{w} \cdot \nabla\xi + \xi\zeta - \nu_\xi \Delta\xi = 0. \tag{3.3}$$

This formulation states roughly that the vorticity is transported by the velocity field and is diffused along time with a diffusion coefficient given by ν_ξ. Compared to the usual 2D vorticity equation, this model includes an additional interaction term between vorticity and divergence. For null divergence, this model comes to the standard vorticity transport equation. Modeling the vorticity divergence product as a zero mean Gaussian random variable, we end up with an imperfect 2D incompressible vorticity-velocity formulation.

Concerning the divergence map, it is more involved to exhibit any conservation law. We will assume here that it behaves like a noise. More precisely we will assume that the divergence map is a function of a Gaussian random variable, X_t, with stationary increments (a Brownian motion) starting at points, x. It can be shown through Ito formula and Kolmogorov's backward equation that the expectation at time t of such a function, $u(t, x) = \mathbb{E}[\zeta(X_t)]$ obeys to a heat equation [28]:

$$\begin{aligned}&\partial_t u - \nu_\zeta \Delta u = 0,\\ &u(0, x) = \zeta(x).\end{aligned} \tag{3.4}$$

[2]A divergence and curl free global transportation component is removed from the vector field. This field is estimated on the basis of a Horn and Schunck estimator associated to a high smoothing penalty [7].

According to this equation, we indeed make the assumption that the divergence at any time of the sequence is a solution of a heat equation (i.e. it can be recovered from a smoothing of the initial motion field divergence map with a Gaussian function of standard deviation $2\sqrt{\nu_\zeta}$).

As the curl and divergence maps completely determine the underlying velocity field, equations (3.3) and (3.4) allow us to write the following imperfect dynamical model for the fluid motion field:

$$\partial_t \begin{bmatrix} \xi \\ \zeta \end{bmatrix}(t) + \underbrace{\begin{bmatrix} \boldsymbol{w}(t)\cdot\nabla\xi(t) + \xi(t)\zeta(t) - \nu_\xi\Delta\xi(t) \\ -\nu_\zeta\Delta\zeta(t) \end{bmatrix}}_{\mathbb{M}(\xi,\zeta,t)} = \nu(t), \tag{3.5}$$

for the state variable (ξ, ζ). The control function $\nu(t)$ is a vector modeling the errors of our evolution law.

3.3. Adjoint model. We now give the adjoint model corresponding to the system of equation (3.5). To obtain this model, we shall first compute the linear tangent operator $\partial_{\boldsymbol{\chi}}\mathbb{M}$, where $\boldsymbol{\chi} = [\xi, \zeta]^T$ denotes the *div-curl* components of the 2D motion field $\boldsymbol{w}$. Introducing the operator K, relation (3.2) can be rewritten as:

$$\boldsymbol{w} = [\nabla^\perp G*, \nabla G*]\boldsymbol{\chi} \triangleq K * \boldsymbol{\chi}. \tag{3.6}$$

The derivation of the system of equation (3.5) with respect to $\boldsymbol{\chi}$ then gives the linear tangent operator $\partial_{\boldsymbol{\chi}}\mathbb{M}$ at point $\boldsymbol{\chi}' = [\xi', \zeta']^T$:

$$\partial_{\boldsymbol{\chi}}\mathbb{M}\boldsymbol{\chi}' = \begin{bmatrix} \boldsymbol{w}\cdot\nabla\xi' + \nabla\xi\cdot(K*\boldsymbol{\chi}') + \zeta\xi' + \zeta'\xi - \nu_\xi\Delta\xi' \\ -\nu_\zeta\Delta\zeta' \end{bmatrix}. \tag{3.7}$$

We can now get $\partial_{\boldsymbol{\chi}}\mathbb{M}^*$, the adjoint operator guiding the adjoint variable $\lambda = [\lambda_\xi, \lambda_\zeta]^T$. Following the definition (2.10), we have:

$$\langle \partial_{\boldsymbol{\chi}}\mathbb{M}\boldsymbol{\chi}', \lambda\rangle = \langle \boldsymbol{\chi}', \partial_{\boldsymbol{\chi}}\mathbb{M}^*\lambda\rangle,$$

the adjoint operator then reads:

$$\partial_{\boldsymbol{\chi}}\mathbb{M}^*\lambda = \begin{bmatrix} \nabla\cdot(\boldsymbol{w}\lambda_\xi) + (\nabla\xi\cdot K*)^*\lambda_\xi + \zeta\lambda_\xi - \nu_\xi\Delta\lambda_\xi \\ \xi\lambda_\xi - \nu_\zeta\Delta\lambda_\zeta \end{bmatrix}. \tag{3.8}$$

However, as some convolution products are involved through the operator K, the formulation of the adjoint member $(\nabla\xi\cdot K*)^*\lambda_\xi$ is not trivial. We know that:

$$\langle \nabla\xi\cdot(K*\boldsymbol{\chi}'), \lambda_\xi\rangle = \langle K*\boldsymbol{\chi}', \nabla\xi\lambda\rangle.$$

Following appendix A, we get:

$$\langle K*\boldsymbol{\chi}', \nabla\xi\lambda\rangle = -\langle \boldsymbol{\chi}', K*(\nabla\xi\lambda)\rangle,$$

so we finally obtain:

$$\partial_{\boldsymbol{\chi}}\mathbb{M}^*\lambda = \begin{bmatrix} \nabla\cdot(\boldsymbol{w}\lambda_\xi) - \nabla^\perp G*(\xi_x\lambda_\xi) + \zeta\lambda_\xi - \nu_\xi\Delta\lambda_\xi \\ -\nabla G*(\xi_y\lambda_\xi) + \xi\lambda_\xi - \nu_\zeta\Delta\lambda_\zeta \end{bmatrix}. \tag{3.9}$$

3.4. Fluid motion observations.

3.4.1. Motion observation model. As a first simple case, we will assume that observation motion fields $\boldsymbol{w}_{obs}(t)$ are available at each image t. This motion field can be provided by any dense motion estimator. In this work, a dense motion field estimator dedicated to fluid flows is used [7]. Referring to equation (3.6), the observation equation is defined as

$$\begin{aligned} Y(t) &= \boldsymbol{w}_{obs}(t) \\ \mathbb{H}_1(\boldsymbol{\chi}, t) &= K * \boldsymbol{\chi}(t). \end{aligned} \tag{3.10}$$

This operator links the motion measurements $\boldsymbol{w}_{obs}$ to the state variable $\boldsymbol{\chi} = [\zeta, \xi]^T$. This observation operator is linear w.r.t $\boldsymbol{\chi}$, so its linear tangent operator is itself:

$$\partial_{\boldsymbol{\chi}} \mathbb{H}_1(\boldsymbol{\chi}', t) = \mathbb{H}_1(\boldsymbol{\chi}', t), \tag{3.11}$$

for a small perturbation $\boldsymbol{\chi}'$. Nevertheless, as this operator is expressed through a convolution product, the expression of its adjoint $\partial_{\boldsymbol{\chi}} \mathbb{H}_1^*$ is not trivial. It is demonstrated in the Appendix A that, under Dirichlet boundaries conditions, it can be expressed as:

$$\partial_{\boldsymbol{\chi}} \mathbb{H}_1^*(\cdot, t) = -\mathbb{H}_1(\cdot, t). \tag{3.12}$$

This first application consists in an oriented smoothing process along a given dynamical law of a sequence of motion fields. As we are only indirectly observing the image data by the way of motion measurements obtained through an external estimation process, we are here dealing with *pseudo-observations*. This situation corresponds to the technique described in [31]. To go further, we now aim at defining a direct relation between the motion fields and the image data.

3.4.2. Image observation model. Starting on the well-known optical flow constraint equation, one can assume, to cope with the aperture problem, that the unknown optic flow vector at a location x is constant within, some neighborhood of size n [24]:

$$g_n * \partial_t I(x, t) + g_n * \nabla I(x, t) \cdot \boldsymbol{w}(x, t) \approx 0, \tag{3.13}$$

where I stands for the luminance function and g_n is a Gaussian window kernel of size n. The system's state $\boldsymbol{\chi}$ is still connected to $\boldsymbol{w}$ through relation (3.6). Hence, our observation system is composed of :

$$\begin{aligned} Y(t) &= g_n * I_t(t), \\ \mathbb{H}_2(\boldsymbol{\chi}, t) &= -g_n * \nabla I(t) \cdot (K * \boldsymbol{\chi}(t)). \end{aligned} \tag{3.14}$$

This observation operator, $\mathbb{H}_2$, is also linear w.r.t the state's variable $\boldsymbol{\chi} = [\zeta, \xi]^T$. Therefore, its linear tangent operator is itself. Following Appendix A, the expression of its adjoint $\partial_{\boldsymbol{\chi}} \mathbb{H}_2^*$, for a small perturbation Y', is given by:

$$\partial_{\boldsymbol{\chi}} \mathbb{H}_2^*(Y', t) = \mathbb{H}_1([g_n * I_x(t) Y', g_n * I_y(t) Y']^T, t).$$

4. Numerical schemes.

4.1. Discretization of the dynamics. The discretization of the vorticity-velocity equation 3.3 must be done cautiously. In particular, the advective term $\nabla \xi \cdot \boldsymbol{w}$ must be treated specifically. A lot of non-oscillatory schemes for conservation laws have been developed to solve this problem [15, 18, 27]. Such schemes consider a polynomial reconstruction of the sought function on cells (here the pixels) and discretize the intermediate value of this function at the cell's boundaries. The involved

derivatives of the transported quantity are computed with high orders accurate difference scheme. The value of these derivatives are attenuated through limiting function (so called slope limiters). This prevents from inappropriate numerical error amplifications. The ENO (Essentially non-oscillatory) or WENO (Weighted ENO) constitute the most used schemes of such family [21, 34].

To achieve an accurate and stable discretization of the advective term, one must use conservative numerical scheme. Such schemes exactly respect the conservation law within the cell by integrating the flux value at cell boundaries. Total Variation Diminishing (TVD) scheme (which are monotonicity preserving flux) prevents from an increase of oscillations over time and enables to transport shocks. All these methods are well detailed in [34].

The time integration is realized with a third-order Runge Kutta scheme, which also respect the TVD property [34]. The divergence is integrated with a stable implicit discretization. The motion field is updated at each time step in the Fourier domain with equation (3.2). With this whole non-oscillatory scheme, the vorticity-velocity and divergence equations can be integrated in the image area. More details about the numerical discretization schemes used in this work can be found in [30].

4.2. Adjoint discretization. Variational data assimilation assumes that the adjoint operator is the exact numerical adjoint of the direct operator [35]. Thus, the adjoint computation must be done according to the previously described vorticity simulation method. For large scale applications involving several coupled state variables of huge dimension and where for each of them a specific dynamical model is discretized accordingly, automatic differentiation programs [13] are used to compute the adjoint model. In our case, as only two variables are involved, it is possible to derive an explicit version of the discretized adjoint operator and a backward Runge-Kutta integration can be realized [14].

5. Results. In this section, we show some experimental results and describe the values we chose for the different parameters. The only parameters of the method are constituted by the covariance matrices associated to the initialization B, the observations $R(t)$ and the dynamical model $Q(t)$. In our applications, we have defined them as diagonals matrices. For the initialization, we systematically imposed $B = 0.1$, the initial condition being provided by an optical flow estimation. Concerning the dynamical model covariance matrix, we fixed it to $Q(t) = 0.01$ for the synthetic sequences, as in this case the dynamic is quasi respected and to $Q(t) = 0.1$ for real world applications with larger dynamical incertitude. The observation covariance matrices are defined with respect to the observation model. In the case of pseudo-observations model (given through dense motion fields provided by optical flow techniques), we fixed the covariance matrix to $R(t) = 0.1$. When observing directly the images, a robust function is introduced to take into account the small gradients of the images:

$$R(x,t) = \alpha(1 - \exp(-||\nabla I(x,t)||)), \qquad \forall x \in \Omega,$$

with $\alpha = 0.1$. For low photometric gradient, the uncertainty value corresponding to the covariance value is automatically set to infinity and as a consequence the associated observation are not taken into account in the estimation. For such points the motion is recovered only through the dynamics.

In order to experimentally assess the benefits of our technique, we first applied it to a synthetic sequence of particles images of a 2D divergence free turbulence obtained by means of a Direct Numerical Simulation (DNS) of the Navier-Stokes equation [5].

For this 52 frames image sequence, we compare in figure 5.1 the actual vorticity maps (line b), the vorticity maps computed by a dedicated optical flow estimator [6, 7](line c), the vorticity maps obtained after assimilating the sequence of motion fields (line d) and the vorticity maps obtained from a direct assimilation (line e).

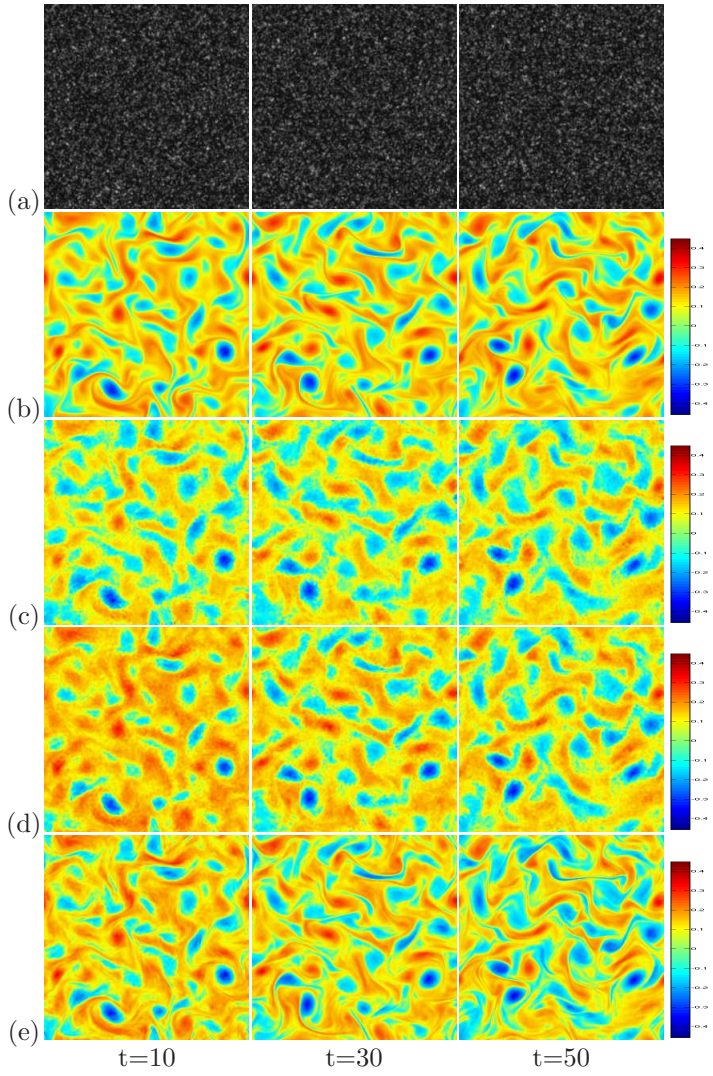

FIG. 5.1. **2D Direct Numerical Simulation, particle sequence**. *Motion observations.* a) *Particle images sequence.* b) *True vorticity.* c) *Vorticity of motion fields provided though the dense technique [6, 7].* d) *Recovered vorticity after assimilating the sequence of motion fields [31].* e) *Vorticity estimated by direct assimilation of the image sequence.*

The filtering technique relying on the assimilation of dense motion fields corresponds to the work presented in [31]. It can be observed that this technique (line d) not only denoises the observations, but also enables to recover small scales structures that were smoothed out in the original velocity fields (line c). These motion fields which constitutes pseudo-observation have been supplied by an external optic flow estimator dedicated to the analysis of fluid flows [6,7]. As can be seen, a direct assimilation of images (line e) performs better than the one based on pseudo-observations.

For this direct assimilation, the quality of the recovered motion field is improved of nearly 30%. To give further quantitative evaluation results, we present the root mean square errors in figures 5.2. In this figure we plotted error measurements corresponding to the motion field supplied by the dense fluid flow dedicated technique [7], the results obtained after assimilating these motion fields and the results provided by a direct assimilation of the image data.

It can also immediately be observed that small motion scales are much better recovered though direct image assimilation. In order to demonstrate this ability more precisely we pictured in figure 5.3, a spectral analysis of the energy of the row average vorticity. This curves show the behavior of the different methods with respect to different frequencies of the flow. We can observe that optical flow measurements are not good for the large and the small motion scales. The assimilation process allows clearly to correct these deficiencies. The direct assimilation fits much accurately the actual curves in the middle scales and in the finest scales.

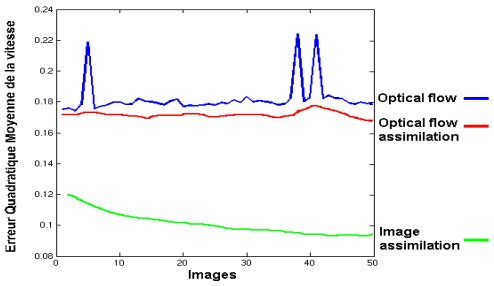

FIG. 5.2. **Particle sequence, Comparison of errors**. *The root mean square error of the motion fields estimated on the sequence are compared for the three methods: fluid dedicated optical flow (in blue) [6, 7], assimilation of optical flow observation (in red) [31] and direct assimilation of image data (in green).*

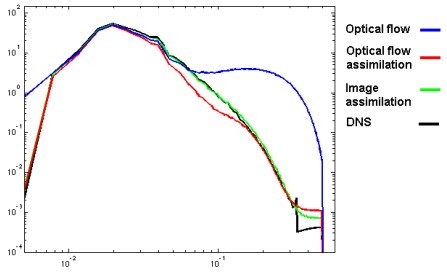

FIG. 5.3. **Particle sequence, spectral analysis** *A spectral analysis of the energy of the row average vorticity is represented in the log-log scale. The actual vorticity (black) is compared to the optical flow vorticity (blue) [6, 7], the vorticity obtained by assimilation of optical flow observation (red) [31] and the one provided by assimilation of image data (green).*

The differences between methods results are even more striking when applying these techniques to a synthetic image sequence representing the diffusion of a passive scalar for the same flow than the previous synthetic example. This sequence is presented in figure 5.4. As can be seen, the images are very smooth (line *a*), and there

is only few areas with significant photometric gradient. Dense motion estimators and correlation techniques provide in this case only very poor results (see line *c*). The assimilation relying on these observations are consequently not satisfying (line *d*). The direct assimilation based on image observations (line *e*) are of much better quality and much closer to the actual values (line *b*).

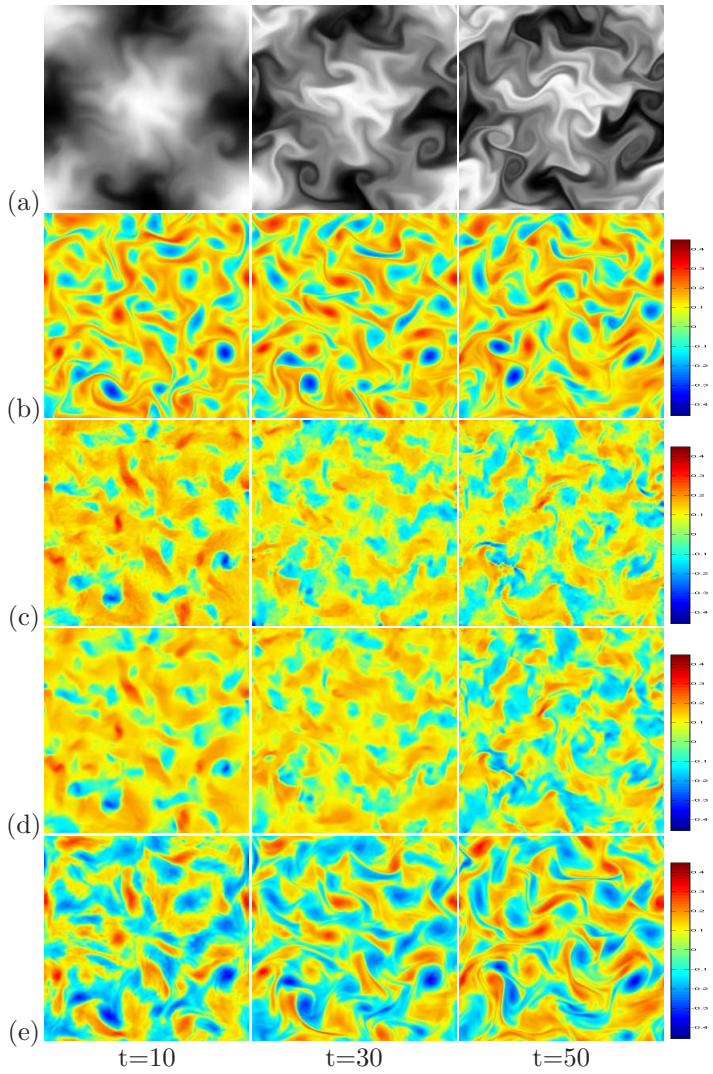

FIG. 5.4. **2D Direct Numerical Simulation, scalar sequence**. a) *Scalar image sequence.* b) *Actual vorticity.* c) *Vorticity observed by optic flow estimator provided through [6, 7].* d) *Vorticity recovered with pseudo-observations.* e) *Vorticity recovered with image observations.*

A quantitative representation of the errors are plotted in figure 5.5 and the corresponding spectral analysis is shown in figure 5.6. It can be check from this latter figure that the results are much better at all scales. The largest structures of the flow and the finest one are nicely reconstructed with the direct assimilation of image data.

Compared to particles images, these images are obviously much closer to the kind of images we have to deal with in environmental sciences. In such domain, the

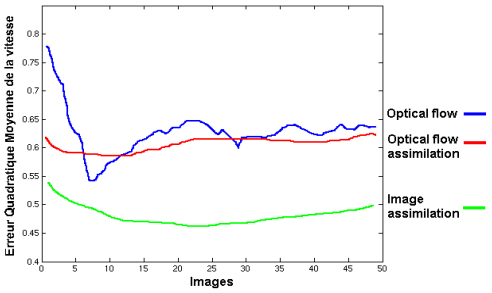

FIG. 5.5. **Scalar sequence, Comparison of errors**. *The root mean square error of the motion fields estimated on the sequence are compared for the three methods: motion fields provided by a fluid flow dedicated optical flow (in blue) [6, 7], the assimilation of optical flow motion fields (in red) [31] and direct assimilation of image data (in green).*

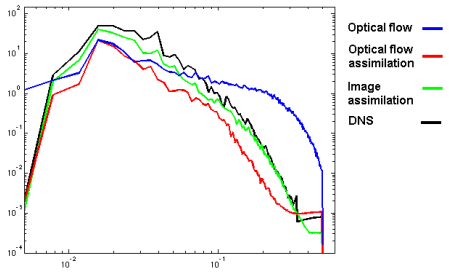

FIG. 5.6. **Scalar sequence, spectral analysis** *A spectral analysis of the energy of the row average vorticity is represented in the log-log scale.The actual vorticity (black) is compared to vorticity of motion field provided by a fluid flow dedicated optical flow estimator (blue) [6, 7], the vorticity obtained after assimilating these noisy motion fields (red) [31] and the one provided by the direct assimilation of image data (green).*

observed scalar consists for instance in plankton concentration in oceanography or temperature in meteorology and oceanography.

To demonstrate the good performances of the direct assimilation technique for environmental sciences applications, we have applied the proposed method on a Meteors satellite meteorological sequence of the Infra-red channel. This sequence describes the evolution of the Vince cyclone over the Atlantic Ocean. This is a 20 frames image sequence shot the 10th of October 2005 from 00H00 to 5H00 by the Meteors Second Generation (MS) satellite. The complete results in terms of vorticity maps are presented in figure 5.7. The use of pseudo-observations (line b) leads to the results presented on line c. When directly considering the images as observations, the resulting vorticity maps are quite different (line d) from the previous ones. We can note however that the cyclone's center and the velocity range are better estimated with the direct method. The method based on pseudo-observation stays more closely to the observed motion field. We can remark that a second counter rotating vortex (blue colored in the top right corner), that was invisible on the motion fields data and which is as a result also missing on the pseudo-observation assimilation results is correctly estimated by the direct assimilation method. This vortex is indeed coherent with respect to cyclone dynamic. For this method we show on figure 5.8, superim-

posed on the original image data, the motion fields recovered. We can checked from these images that the motion of the cyclone's eye is very well recovered. This last results illustrate the fact that the estimations provided are coherent with respect to the visualized phenomenon.

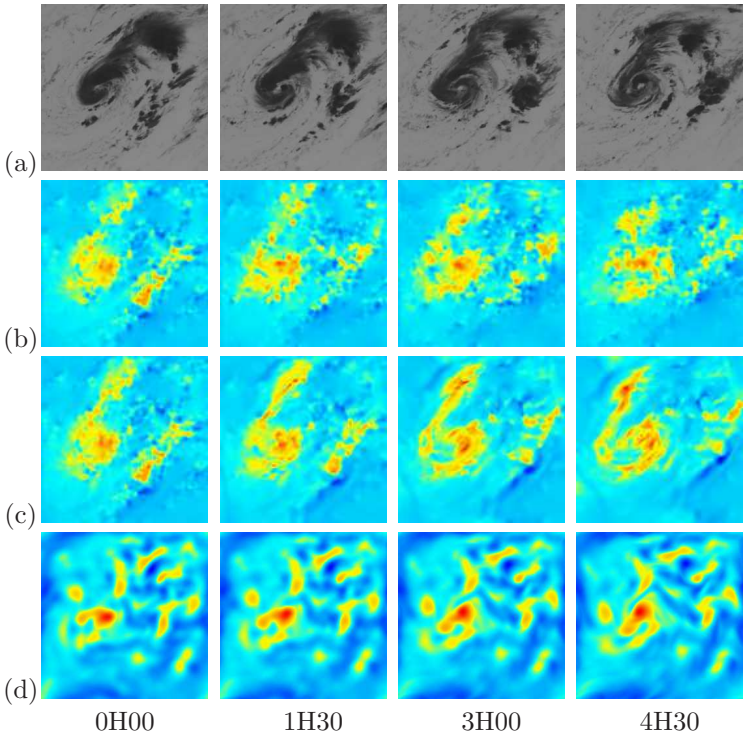

FIG. 5.7. **Vince cyclone**. (a) *Infra-red image sequence.* (b) *Vorticity maps of the motion fields provided by a fluid flow dedicated technique [6, 7].* (c) *Vorticity maps obtained after the assimilation of these motion fields [31].* (d) *Vorticity maps obtained through the direct assimilation of the infra-red channel image sequence.*

In order to demonstrate the validity of the dynamics we used and also the robustness the method, we now consider the *visible channel* image sequence of the MS satellite depicting at the same moment the Vince cyclone. This sequence corresponds to 24 hours cyclone's evolution. Observations are only available during the day and are missing from the 9th of October 19H00 to the 10th of October 8H00. During this time interval, the corresponding covariance matrices $R(t)$ are automatically set to infinity as no photometric contrast are observed. The assimilation results are plotted in terms of velocity fields and are superimposed on the *infra-red images* in the figure A.1 in order to assess the quality of the measurements. We can evaluate visually the quality of the estimations. As the cyclone increased its speed during the night, the estimation is not perfect. It nevertheless demonstrates that the approximate motion dynamics used in the previous example reveals to be quite good as it allows to reconstructed the cyclone dynamics despite a very large occlusion.

6. Conclusion. In this work, a variational framework for the tracking of fluid flows has been introduced. This approach relies on variational data assimilation principles. The proposed method allows to recover the state of an unknown function on the basis of an imperfect dynamical model and noisy measurement of this function.

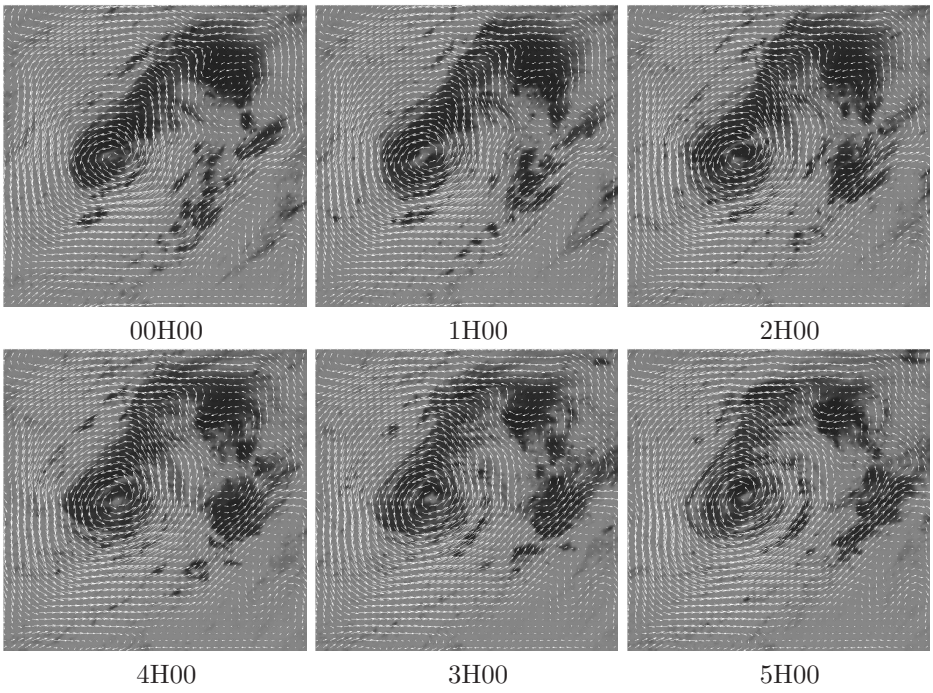

FIG. 5.8. **Cyclone Vince**. *Motion fields recovered from the direct assimilation of the Infra-red channel image sequence.*

These basic ingredients of the technique have been tested on synthetic sequence and applied to the tracking of fluid motion on real image sequences. Thanks to the dynamics, such an approach allows estimating dense motion field without introducing spatial regularization constraints.

To go further, it could be interesting to introduce accurate dynamic laws more precisely related to the observed phenomenon and to couple eventually direct assimilation of image data and pseudo-observation. The tuning and the balance of the corresponding covariance matrices is however an intricate issue and we wished in this paper to focus explicitly on the methodology and on the differences brought by these two different assimilation strategies. We have applied these techniques to fluid motion, nevertheless we believe that considering sound adaptations, it could be considered for various applications of computer vision. Such framework could certainly be considered with great benefits for video restoration, image measurement in noisy contexts (echographic images for instance), or motion estimation of occluded object.

Acknowledgments. The authors would like to thank the Cemagref laboratory and the Laboratoire de Météorologie Dynamique for providing the image sequences presented in this paper. This work was supported by the European Community through the IST FET Open FLUID project (`http://fluid.irisa.fr`).

Appendix A. Green kernel adjoint operator. The analytic form of the adjoint observation operator involved in equation 3.12 is here demonstrated. In order to have more compact notations, let $\boldsymbol{Z}(x) = [\Psi(x), \Phi(x)]^T$ denotes the *potential coordinates*. These coordinates are linked to the *div-curl coordinates*, $\boldsymbol{\chi}(x) = [\xi(x), \zeta(x)]^T$ through the relations (3.1):

$$\boldsymbol{Z} = G * \boldsymbol{\chi}. \tag{A.1}$$

Besides, relation (3.2) reads immediately:

$$u = \nabla^{\perp} \cdot \boldsymbol{Z} \qquad \text{and} \qquad v = \nabla \cdot \boldsymbol{Z}. \tag{A.2}$$

As previously, the vector field $\boldsymbol{Z}$ may be written on the basis of the Helmholtz decomposition as the sum of the gradient of two scalar functions. Relation (A.2) allows us to write both motion components as solutions of two Poisson equations. Expressing these solutions through Green kernel enables to write the vector field $\boldsymbol{Z}$ as:

$$\boldsymbol{Z} = \nabla^{\perp} G * u + \nabla G * v = K * \boldsymbol{w}. \tag{A.3}$$

It can be can noticed that the same operator is involved in (3.2) and (A.3), indeed:

$$\boldsymbol{w} = \nabla^{\perp} G * \xi + \nabla G * \zeta = K * \boldsymbol{\chi}. \tag{A.4}$$

These last notations, which link the stream function and the velocity potential to the vector field, will be useful in the following.

PROPOSITION A.1. *Let $\boldsymbol{w}^A$ and $\boldsymbol{w}^B$ be two vector fields belonging to $C^2(\Omega) \cap L^2(\Omega)$, where Ω is a bounded set of $\mathbb{R}^2$ with border $\partial\Omega$. Assuming that the components of both vector fields admit Dirichlet boundaries conditions, i.e $u^{A,B}|_{\partial\Omega} = v^{A,B}|_{\partial\Omega} = 0$, then $\langle \boldsymbol{w}^A, \boldsymbol{w}^B \rangle = -\langle \boldsymbol{Z}^A, \boldsymbol{\chi}^B \rangle = -\langle \boldsymbol{\chi}^A, \boldsymbol{Z}^B \rangle$.*

Proof.

$$\begin{aligned}
\left\langle \boldsymbol{w}^A, \boldsymbol{w}^B \right\rangle &\overset{(A.2)}{=} \begin{bmatrix} u^A \\ v^A \end{bmatrix} \cdot \begin{bmatrix} \nabla^{\perp} \cdot \boldsymbol{Z}^B \\ \nabla \cdot \boldsymbol{Z}^B \end{bmatrix} \\
&= u^A(\Phi^B_x - \Psi^B_y) + v^A(\Phi^B_y + \Psi^B_x) \\
&= -\Psi^B(v^A_x - u^A_y) - \Phi^B(u^A_x + v^A_y) + \underbrace{\text{Boudary terms}}_{=0} \\
&= -\left\langle \boldsymbol{\chi}^A, \boldsymbol{Z}^B \right\rangle.
\end{aligned}$$

□

We thus proved that $\left\langle \boldsymbol{w}^A, K * \boldsymbol{\chi}^B \right\rangle = -\left\langle K * \boldsymbol{w}^A, \boldsymbol{\chi}^B \right\rangle$, so:

$$(K*)^* = -K*.$$

REFERENCES

[1] A.F. BENNET, *Inverse Methods in Physical Oceanography*, Cambridge University Press, 1992.

[2] M. BLACK AND P. ANANDAN, *Robust dynamic motion estimation over time*, in Proc. IEEE Comput. Vis. and Pat. Rec. CVPR'92, 1991, pp. 296–302.

[3] A. BORZÌ, K. ITO, AND K. KUNISCH, *Optimal control formulation for determining optical flow*, SIAM Journal on Scientific Computing, 24 (2003), pp. 818–847.

[4] T. BROX, A. BRUHN, N. PAPENBERG, AND J. WEICKERT, *High accuracy optical flow estimation based on a theory for warping*, in Proc. Europ. Conf. Comput. Vis., ECCV'04, Prague, Czech Republic, 2004, Springer–Verlag, pp. 25–36.

[5] J. CARLIER AND B. WIENEKE, *Report on production and diffusion of fluid mechanics images and data*, tech. report, Fluid Project deliverable 1.2, 2005.

[6] T. CORPETTI, D. HEITZ, G. ARROYO, É MÉMIN, AND A. SANTA-CRUZ, *Fluid experimental flow estimation based on an optical-flow scheme*, Int. J. Experiments in Fluid, 40 (2006), pp. 80–97.

[7] T. CORPETTI, É. MÉMIN, AND P. PÉREZ, *Dense estimation of fluid flows*, IEEE Trans. Pat. Anal. Mach. Intell., 24 (2002), pp. 365–380.

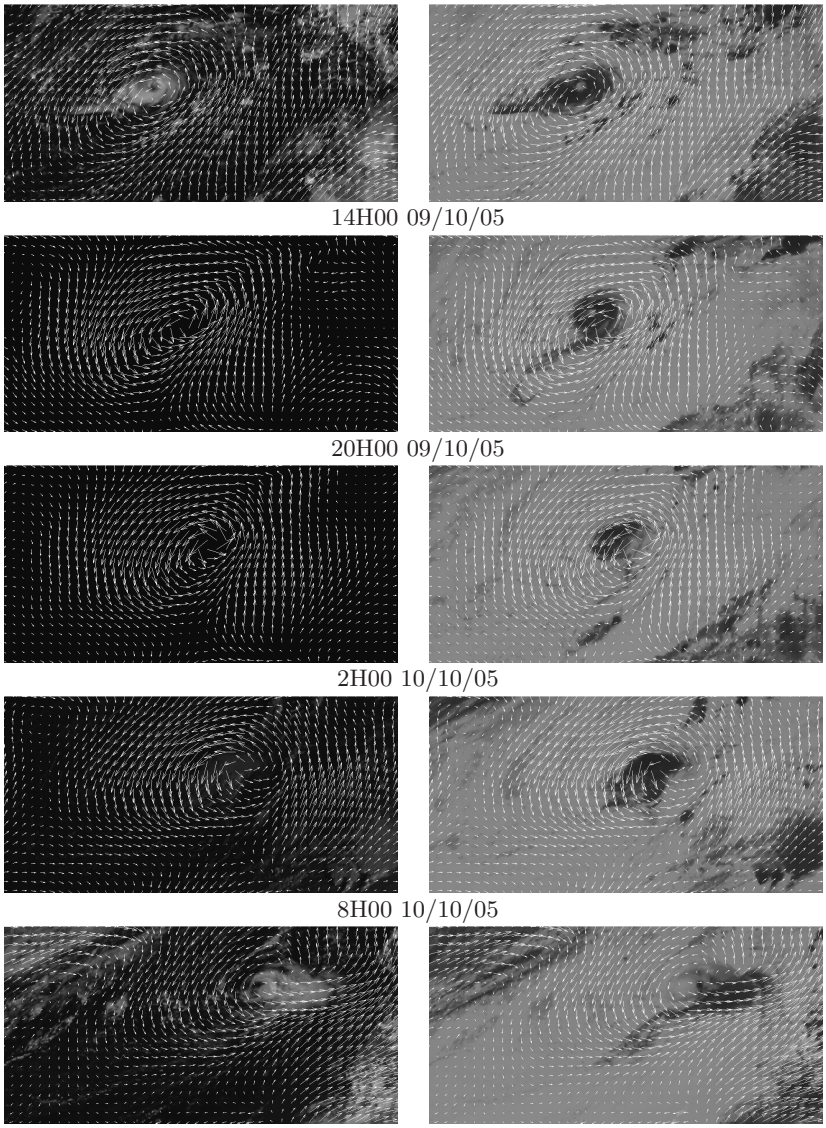

FIG. A.1. **Vince cyclone tracked by night**. *The motion fields obtained from the assimilation of the pseudo-observations computed with the* visible images *are superimposed: (a) on these* visible images*, (b) on the* infra-red images. *There is a data occlusion from the 9th of October at 19H00 to the 10th of October at 8H00. As there is no observations on the three central images on the visible channel, the velocities estimations of the cyclone eye are not perfect.*

[8] ———, *Extraction of singular points from dense motion fields: an analytic approach*, J. Math. Imaging and Vision, 19 (2003), pp. 175–198.

[9] A. CUZOL, P. HELLIER, AND É. MEMIN, *A low dimensional fluid motion estimator*, Int. J. Comput. Vis., 75 (2007), pp. 329–349.

[10] A. CUZOL AND É. MÉMIN, *A stochastic filter for fluid motion tracking*, in Proc. IEEE Int. Conf. Comput. Vis., ICCV'05, vol. 1, Beijing, China, October 2005, pp. 396–402.

[11] J.M. FITZPATRICK, *A method for calculating velocity in time dependent images based on the continuity equation*, in Proc. IEEE Comput. Vis. and Pat. Rec. CVPR'95, San Francisco, USA, 1985, pp. 78–81.

[12] R.M. Ford, R. Strickland, and B. Thomas, *Image models for 2-d flow visualization and compression*, Graph. Mod. Image Proc., 56 (1994), pp. 75–93.
[13] R. Giering and T. Kaminski, *Recipes for adjoint code construction*, ACM Trans. Math. Softw., 24 (1998), pp. 437–474.
[14] M. Giles, *On the use of runge-kutta time-marching and multigrid for the solution of steady adjoint equations*, Tech. Report 00/10, Oxford University Computing Laboratory, 2000.
[15] A. Harten, B. Engquist, S. Osher, and S. R. Chakravarthy, *Uniformly high order accurate essentially non-oscillatory schemes, 111*, J. of Comput. Phys., 71 (1987), pp. 231–303.
[16] P. Héas, E. Mémin, N. Papadakis, and A. Szantai, *Layered estimation of atmospheric mesoscale dynamics from satellite imagery*, IEEE Trans. Geoscience and Remote Sensing, 45 (2007), pp. 4087–4104.
[17] T. Kohlberger, É. Mémin, and C. Schnörr, *Variational dense motion estimation using the helmholtz decomposition*, in Proc. Int. Conf. on Scale-Space and PDE methods in Comput. Vis., Scale-Space'03, Isle of Skye, UK, 2003, pp. 432–448.
[18] A. Kurganov and E. Tadmor, *New high-resolution central schemes for nonlinear conservation laws and convetion-diffusion equations*, J. of Comput. Phys., 160 (2000), pp. 241–282.
[19] R. Larsen, K. Conradsen, and B.K. Ersboll, *Estimation of dense image flow fields in fluids*, IEEE trans. on Geosc. and Remote sensing, 36 (1998), pp. 256–264.
[20] F.-X. Le Dimet and O. Talagrand, *Variational algorithms for analysis and assimilation of meteorological observations: theoretical aspects*, Tellus, 38 (1986), pp. 97–110.
[21] D. Levy, G. Puppo, and G. Russo, *A third order central weno scheme for 2d conservation laws*, Appl. Num. Math.: Trans. of IMACS, 33 (2000), pp. 415–421.
[22] J. Lions, *Contrôle optimal de systèmes gouvernés par des équations aux dérivées partielles*, Dunod, 1968.
[23] J.L. Lions, *Optimal control of systems governed by PDEs*, Springer-Verlag, New York, 1971.
[24] B. Lucas and T. Kanade, *An iterative image registration technique with an application to stereovision*, in Int. Joint Conf. on Artificial Intel. (IJCAI), 1981, pp. 674–679.
[25] E. Mémin and P. Pérez, *Fluid motion recovery by coupling dense and parametric motion fields*, in Proc. IEEE Int. Conf. Comput. Vis., ICCV'99, 1999, pp. 620–625.
[26] H.H. Nagel, *Extending the oriented smoothness constraint into the temporal domain and the estimation of derivatives of optical flow*, in Proc. Europ. Conf. Comput. Vis., ECCV'90, Antibes, France, Apr 1990, Springer, pp. 139–148.
[27] H. Nessyahu and E. Tadmor, *Non-oscillatory central differencing for hyperbolic conservation laws*, J. of Comput. Phys., 87 (1990), pp. 408–463.
[28] B. Oksendal, *Stochastic differential equations*, Spinger-Verlag, 1998.
[29] N. Papadakis, T. Corpetti, and É. Mémin, *Dynamically consistent optical flow estimation*, in Proc. IEEE Int. Conf. Comput. Vis., ICCV'07, Rio de Janeiro, Brasil, October 2007.
[30] N. Papadakis and É. Mémin, *A variational framework for spatio-temporal smoothing of fluid motions*, in Proc. Scale Space and Variational Methods, SSVM'07, Ischia, Italy, May 2007, pp. 603–615.
[31] N. Papadakis and É. Mémin, *A variational technique for joint tracking of curve and motion*, J. Math. Imaging and Vision, 31 (2008), pp. 81–103.
[32] P. Ruhnau and C. Schnörr, *Optical stokes flow estimation: An imaging-based control approach*, Exp.in Fluids, 42 (2007), pp. 61–78.
[33] P. Ruhnau, A. Stahl, and C. Schnörr, *Variational estimation of experimental fluid flows with physics-based spatio-temporal regularization*, Meas. Sci. Technol., 18 (2007), pp. 755–763.
[34] C.-W. Shu, *Advanced Numerical Approximation of Nonlinear Hyperbolic Equations, Lecture Notes in Mathematics*, vol. 1697, Springer Berlin, 1998, ch. Essentially non-oscillatory and weighted essentially non-oscillatory schemes for hyperbolic conservation laws, pp. 325–432.
[35] O. Talagrand, *Variational assimilation. Adjoint equations*, Kluwer Academic Publishers, 2002.
[36] O. Talagrand and P. Courtier, *Variational assimilation of meteorological observations with the adjoint vorticity equation. I: Theory*, Q. J. Roy. Meteorol. Soc., 113 (1987), pp. 1311–1328.
[37] J. Weickert and C. Schnörr, *Variational optic-flow computation with a spatio-temporal smoothness constraint*, J. Math. Imaging and Vision, 14 (2001), pp. 245–255.
[38] J. Yuan, C Schnörr, and É. Mémin, *Discrete orthogonal decomposition and variational fluid flow estimation*, J. Math. Imaging and Vision, 28 (2007), pp. 67–80.
[39] L. Zhou, C. Kambhamettu, and D. Goldgof, *Fluid structure and motion analysis from multi-spectrum 2D cloud images sequences*, in Proc. IEEE Comput. Vis. and Pat. Rec. CVPR'00, vol. 2, Hilton Head Island, USA, 2000, pp. 744–751.